

Article

Metal-Free Phosphination and Continued Functionalization of Pyridine: A Theoretical Study

Pan Du ¹, Yuhao Yin ², Dai Shi ², Kexin Mao ², Qianyuan Yu ² and Jiyang Zhao ^{2,*} ¹ School of Life Science and Chemistry, Jiangsu Second Normal University, Nanjing 210013, China² School of Environmental Science, Nanjing Xiaozhuang University, Nanjing 211171, China

* Correspondence: jyzhao1981@163.com

Abstract: This study investigates the mechanism of metal-free pyridine phosphination with P(OEt)₃, PPh₃, and PAr₂CF₃ using density functional theory calculations. The results show that the reaction mechanism and rate-determining step vary depending on the phosphine and additive used. For example, phosphination of pyridine with P(OEt)₃ occurs in five stages, and ethyl abstraction is the rate-determining step. Meanwhile, 2-Ph-pyridine phosphination with PPh₃ is a four-step reaction with proton abstraction as the rate-limiting step. Energy decomposition analysis of the transition states reveals that steric hindrance in the phosphine molecule plays a key role in the site-selective formation of the phosphonium salt. The mechanism of 2-Ph-pyridine phosphination with PAr₂CF₃ is similar to that with PPh₃, and analyses of the effects of substituents show that electron-withdrawing groups decreased the nucleophilicity of the phosphine, whereas aryl electron-donating groups increased it. Finally, TfO[−] plays an important role in the C–H fluoroalkylation of pyridine, as it brings weak interactions.

Keywords: phosphination; metal free; C–H fluoroalkylation; mechanism; DFT

Citation: Du, P.; Yin, Y.; Shi, D.; Mao, K.; Yu, Q.; Zhao, J. Metal-Free Phosphination and Continued Functionalization of Pyridine: A Theoretical Study. *Molecules* **2022**, *27*, 5694. <https://doi.org/10.3390/molecules27175694>

Academic Editor: Maxim L. Kuznetsov

Received: 10 August 2022

Accepted: 31 August 2022

Published: 3 September 2022

Publisher's Note: MDPI stays neutral with regard to jurisdictional claims in published maps and institutional affiliations.

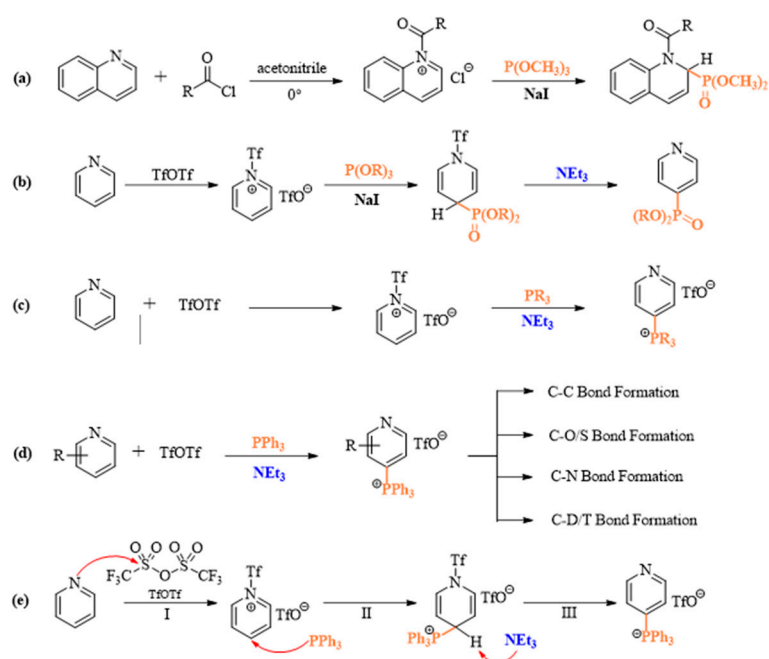


Copyright: © 2022 by the authors. Licensee MDPI, Basel, Switzerland. This article is an open access article distributed under the terms and conditions of the Creative Commons Attribution (CC BY) license (<https://creativecommons.org/licenses/by/4.0/>).

1. Introduction

Organophosphorous compounds have broad applications in the fields of organic synthesis, ligand chemistry, medicinal chemistry, agrochemistry, and materials [1–3]. In light of their fundamental importance, many methods of C–P bond formation have been developed [4–6]. Among these methods, transition-metal-catalyzed cross-coupling reactions, including the Pd- [7], Cu- [8], Zn- [9], Ni- [10], Mn- [11], Ag- [12], and Rh-catalyzed [13] phosphination reactions of various aryl partners with phosphine reagents, have received great attention [14]. In particular, researchers have focused on developing a mild, efficient, and environmentally benign method of C–P bond formation [15–17].

In 1979, the Akiba group succeeded in synthesizing dimethyl phosphonates by reacting quinoline or isoquinoline with acyl chlorides then adding trimethyl phosphite (Scheme 1a) [18]. Since then, many improved methods have been developed. For example, Ander et al. reported the synthesis of PO(OR)₂- and PR₃-substituted N-heteroaromatic rings by reaction of the N-heteroaromatic ring with phosphorous compounds in the presence of Tf₂O and amine (Scheme 1b,c) [19–23]. Although the formation of metal-free C–P bonds has been investigated for many decades, little progress had been made in this area until McNally and co-workers finally succeeded in developing a general approach to form C–O, C–S, C–C, C–D/T, and C–N bonds by transforming pyridines to phosphonium salts then reacting them with nucleophiles (Scheme 1d) [24–32]. The groups of Harutyunyan and Jumde were able to produce pyridyl-ether by directly functionalizing the pyridine ring according to the methodology proposed by McNally and co-workers [33]. The metal-free Sandmeyer-type phosphorylation of aryl amines and electrophilic phosphinative cyclization of alkynes were used to synthesize aryl phosphonates [34] and various phosphine derivatives [35]. Finally, Stephan et al. used Frustrated Lewis Pairs to form compounds with C–P bonds [36].



Scheme 1. (a–d) Phosphination reaction of pyridine derivatives with different phosphorous compounds. (e) Proposed mechanism of C–P bond formation.

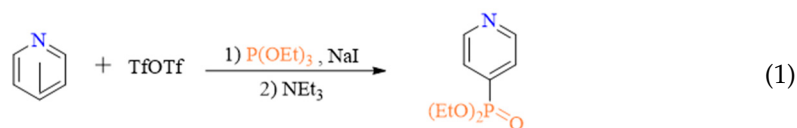
Despite their importance for the construction of phosphorous compounds and phosphonium salts, which can be used as a late-stage functionalization tool, the mechanisms underlying the formation of metal-free C–P bonds are not well understood. McNally et al. proposed a possible reaction pathway for the reaction illustrated in Scheme 1c, as shown in Scheme 1e [27]. According to this mechanism, the reaction is initiated by the nucleophilic attack of pyridine on Tf_2O (I) to form a pyridinium triflyl salt. The addition of phosphine to this salt results in the formation of a C–P bond (II). In the last step, the NEt_3 base abstracts an H-atom from the adduct to restore aromaticity (III). Although this mechanism explains how the C–P bond is formed, it does not account for the factor controlling the site-selective formation of the phosphonium salt. In reaction Scheme 1b, NaI is involved in the generation of the C–P bond, and the product is neutral. Meanwhile, in reaction Scheme 1c, the product is an ion pair. The role of NaI and the reason behind the difference in product nature remain unclear. In this study, we investigate the detailed mechanisms of pyridine reaction with $\text{P}(\text{OEt})_3$, PPh_3 , and PAR_2CXF_2 phosphines, and we assess the effect of the phosphine on the formation of metal-free C–P bonds.

2. Results and Discussion

In this section, we discuss the possible mechanisms of pyridine phosphination with $\text{P}(\text{OEt})_3$, PPh_3 , and PAR_2CXF_2 . The site-selectivity of the reaction is also analyzed.

2.1. Mechanism of Pyridine Phosphination with $\text{P}(\text{OEt})_3$

The computed Gibbs free energy profiles corresponding to the phosphination of pyridine with $\text{P}(\text{OEt})_3$ in acetonitrile solvent (Equation (1)) are presented in Figures 1 and 2. The optimized geometries of all stationary points along the reaction pathway are displayed in Figures S1 and S2 of the Supplementary Materials.



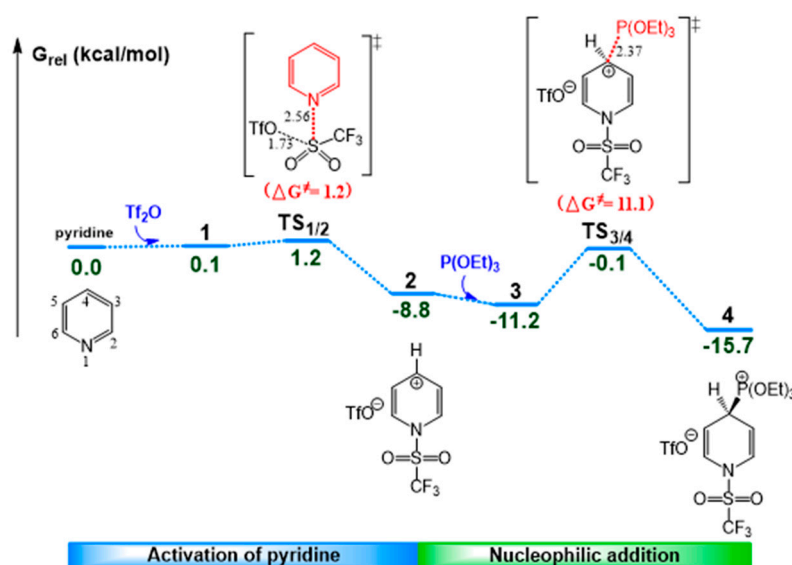


Figure 1. Free energy profile of pyridine activation and nucleophilic addition.

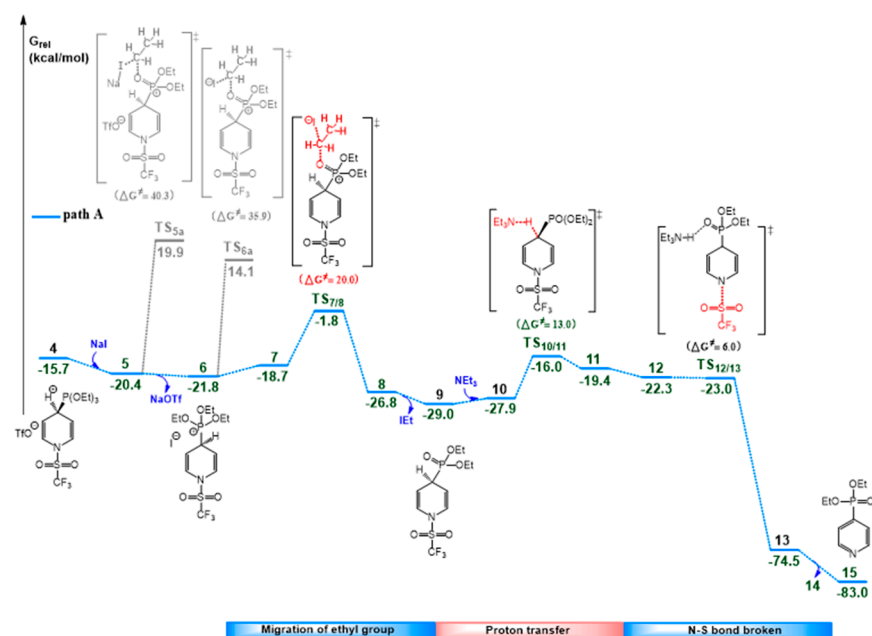


Figure 2. Free energy profile of dihydropyridine rearomatization to afford the final product (path A).

2.1.1. Activation of Pyridine and Nucleophilic Addition

Based on our calculations, the reaction is initiated by the nucleophilic attack of pyridine on Tf_2O (S_N2 reaction) to form N -(trifluoromethylsulfonyl)pyridinium triflate **2** and TfO^- via the $TS_{1/2}$ transition state [37]. The free energy barrier of this reaction step is only 1.2 kcal/mol in acetonitrile (relative to pyridine + Tf_2O), which agrees well with the expected barrier value, considering the experimental conditions ($-78^\circ C$ to room temperature). The $S-O(OTf)$ bond in $TS_{1/2}$ is elongated to 1.73 Å, whereas the $N-S$ bond distance is decreased to 2.56 Å. The natural population analysis (NPA) charge of the C4 atom of the pyridine moiety increases from -0.159 in free pyridine to -0.06 in intermediate **2**, which indicates that this atom becomes more electrophilic along the reaction pathway. Therefore, Tf_2O facilitates the nucleophilic addition reaction by strengthening the electrophilicity of pyridine.

The second reaction step involves the addition of the phosphine $P(OEt)_3$ nucleophile to intermediate **2** via the $TS_{3/4}$ transition state, yielding N -trifluoromethylsulfonyldihydropyridine

4. This step has a free energy barrier of 11.1 kcal/mol in acetonitrile (relative to 3), which is relatively low, and the C4–P bond distance in $TS_{3/4}$ is 2.37 Å. The approach of $P(OEt)_3$ distorts the pyridine ring, and in the dearomatized intermediate 4, this ring has a typical dihydropyridine structure.

2.1.2. Rearomatization of Dihydropyridine

The rearomatization of dihydropyridine (intermediate 4) occurs via two possible reaction pathways. The first pathway involves the NaI-mediated migration of an ethyl group, followed by proton abstraction by NEt_3 (path A in Figure 2). Meanwhile, in the second pathway, abstraction occurs first, then migration (path B in Figure 3).

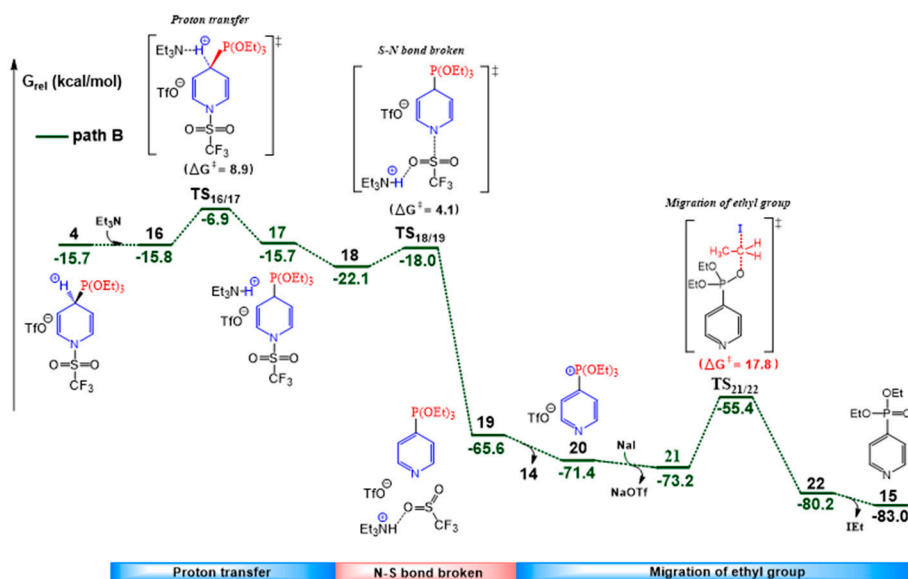


Figure 3. Free energy profile of dihydropyridine rearomatization to afford the final product (path B).

As shown in Figure 2, path A of dihydropyridine rearomatization is mediated by NaI, which can directly extract the ethyl group in 4 via TS_{5a} . However, the free energy barrier of this step is high (40.3 kcal/mol). Alternatively, the TfO^- ion in 4 may be exchanged with the I^- ion of NaI, which promotes the migration of the ethyl group. The iodide ion may attack the ethyl groups from the frontside via TS_{6a} or from the backside via $TS_{7/8}$, with free energy barriers of 35.9 and 20.0 kcal/mol, respectively. The attack of I^- on the ethyl groups is an S_N2 type reaction, where the iodide ion acts as a nucleophile. Considering that the attack of I^- from the backside yields higher orbital overlap than the attack from the frontside (Figure 4), $TS_{7/8}$ is more favorable than TS_{5a} or TS_{6a} .

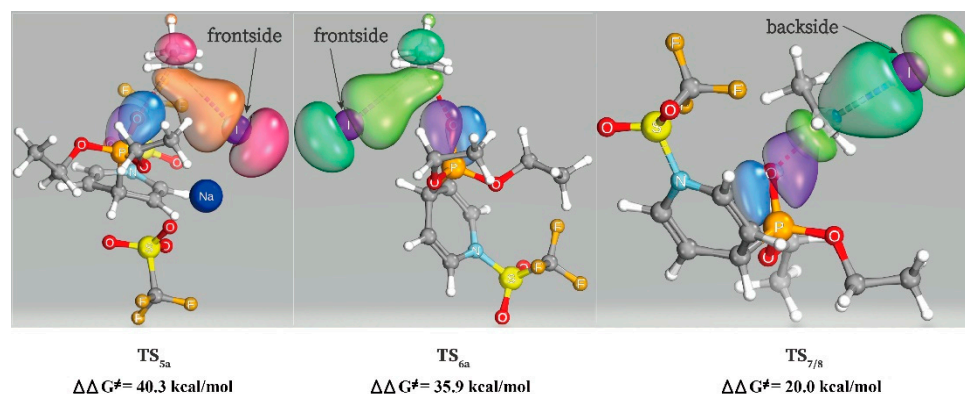


Figure 4. Orbital interactions implicated in the three S_N2 transition states: TS_{5a} , TS_{6a} , and $TS_{7/8}$.

Subsequently, the product of the S_N2 reaction, 4-Phosphonato substituted pyridine **9**, reacts with NEt_3 to generate intermediate **11** via a proton transfer transition state ($TS_{10/11}$). With a free energy barrier of 13.0 kcal/mol only (relative to **9**), this reaction step occurs readily. Intermediate **11** undergoes isomerization to a more stable isomer **12**, in which the ammonium cation is close to the P=O group. Then, the N-S bond in **12** breaks to form intermediate **13** via $TS_{12/13}$, which lies at 6.0 kcal/mol above **9**. The final product **15** is obtained upon the dissociation of the $Et_3HN^+ \cdots CF_3SO_2^-$ ion pair **14** from **13**.

In path B, proton abstraction precedes the migration of the ethyl group. The free energy profile of this pathway is shown in Figure 3, and the optimized geometries of all implicated species are given in Figure S3. First, the NEt_3 amine abstracts a proton from the C4 of the dihydropyridine intermediate **4** via $TS_{16/17}$ to generate intermediate **17**. The free energy barrier of this process is 8.9 kcal/mol (relative to **4**), which is relatively low. Then, intermediate **17** isomerizes to a more stable isomer **18**, in which the ammonium cation is close to the Tf group. Subsequently, the N-S bond in **18** breaks, resulting in the formation of intermediate **19** via $TS_{18/19}$, which lies at 4.1 kcal/mol above **18**. Finally, the iodide ion of NaI abstracts the ethyl group of **19** via an S_N2 reaction, whose free energy barrier is only 17.8 kcal/mol ($TS_{21/22}$). This indicates that the I^- -mediated migration of the ethyl group is a facile process. In both paths, A and B, ethyl migration is the rate-determining step. The free energy barrier of this step in path B is 17.8 kcal/mol ($TS_{21/22}$), which is comparable to that in path A ($TS_{7/8}$, 20.0 kcal/mol). This reveals that the reaction can also occur when the order of the addition of NaI and NEt_3 in the experiment is reversed.

Overall, our calculations suggest that path A (i.e., the activation of pyridine and nucleophilic addition of $P(OEt)_3$, followed by the migration of the ethyl group and rearomatization of dihydropyridine) is energetically feasible, with an overall energy change of -83.0 kcal/mol. The rate-limiting step is the nucleophilic addition of $P(OEt)_3$ via $TS_{7/8}$, which has a free energy barrier of 20.0 kcal/mol. Although the order of the elementary steps is reversed in path B, this path can also occur under experimental conditions.

2.1.3. Origin of Site-Selectivity

Based on the experiments conducted in a previous study, the reaction of pyridine with $P(OEt)_3$ results in the nearly exclusive formation of C4-phosphonates (C4-phosphonate:C2-phosphonate = 95:5) [22]. The implicated mechanism of the formation of C2-phosphonate involves nucleophilic addition ($o-TS_{3/4}$, 13.7 kcal/mol) and the migration of the ethyl group ($o-TS_{7/8}$, 21.9 kcal/mol), as illustrated in Figure 5. The rate-determining step is ethyl group abstraction by I^- ($o-TS_{7/8}$). Notably, C2-phosphonates may be formed via the same mechanism as C4-phosphonates; however, the free energy barriers of the key reaction steps are lower in the case of C4-phosphonate formation, as shown in Table 1. Moreover, the energy of the C4-phosphonate product is lower than that of the C2 counterpart. These results indicate that compared to C2-phosphonate formation, the production of C4-phosphonates is more favored both dynamically ($TS_{3/4}$ and $TS_{7/8}$) and thermodynamically (**9**).

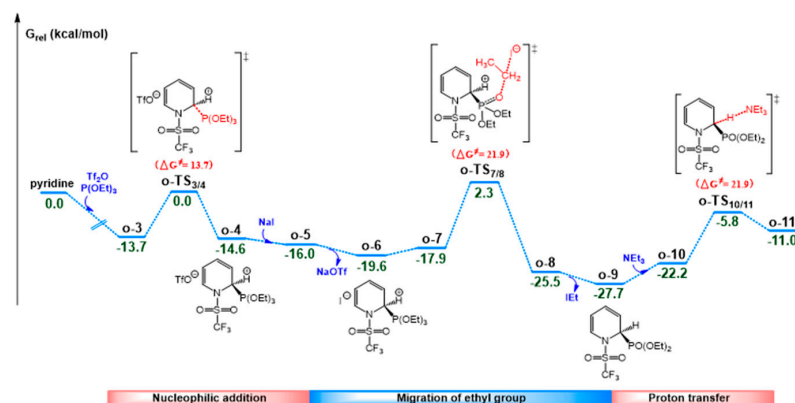


Figure 5. Free energy profile of pyridine phosphonation to afford C2-phosphonates.

Table 1. The free energy barriers of key elementary reactions and energies of the C2- and C4-phosphonate products (unit kcal/mol).

	TS _{3/4}	TS _{7/8}	Product (9)
Formation of C4-phosphonate	11.1	20.0	−27.2
Formation of C2-phosphonate	13.7	21.9	−25.9

The C2-phosphonate **o-9** undergoes proton abstraction by NEt₃ via the **o-TS_{10/11}** transition state. The related free energy barrier is 21.9 kcal/mol, compared with 13.1 kcal/mol for proton abstraction from the C4-phosphonate (**TS_{10/11}**). Considering the relatively high barrier of **o-9** rearomatization, this is the main product of the reaction.

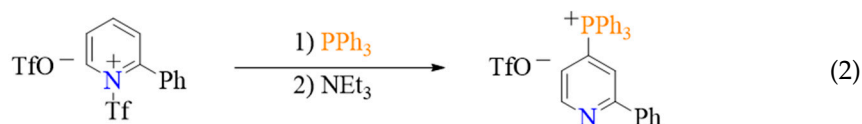
To determine the origin of product selectivity, activation strain model (ASM) [38–40] analyses of the **TS_{7/8}** and **o-TS_{7/8}** transition states were conducted. These transition states may be divided into two parts, one involving phosphorane and I[−], and the other involving pyridine and the Tf group. The energy of the interaction between the two parts in **TS_{7/8}** and **o-TS_{7/8}** is −106.9 and −113.5 kcal/mol, respectively. The larger interaction energy of **o-TS_{7/8}** compared to **TS_{7/8}** is attributed to the presence of a strong π bond in the former. As for the strain energies of the phosphorane and pyridine moieties, they are larger in **o-TS_{7/8}** than in **TS_{7/8}** (Table 2), which indicates that the steric hindrance in the former is greater than that in the latter. Considering that the interaction energy and strain energy differences between **TS_{7/8}** and **o-TS_{7/8}** are −6.6 and 10.8 kcal/mol, respectively, the free energy of **o-TS_{7/8}** is larger than that of **TS_{7/8}**, and the para-substituted phosphonate is the main product. In summary, the product selectivity is determined by the steric hindrance. The phosphination of pyridine with P(O*t*Pr)₃ to afford C2- and C4-phosphonates was also explored, and the results confirm that steric hindrance plays a key role in site-selectivity. The related free energy profiles and optimized structures are presented in Figures S5–S8.

Table 2. Interaction and strain energies of the **TS_{7/8}** and **o-TS_{7/8}** transition states (unit kcal/mol).

	E _{inter}	E _{strain}		
		Phosphonate	Pyridine	Sum
TS_{7/8}	−106.9	59.8	46.1	105.9
o-TS_{7/8}	−113.5	67.9	48.8	116.7
differ	−6.6	8.1	2.7	10.8

2.2. Phosphination of Pyridine with PPh₃

2.2.1. Mechanism of Pyridine Phosphination with PPh₃



As there is no NaI additive, the process of 2-Ph-pyridine phosphination with PPh₃ is simpler than that with P(OEt)₃ (Equation (2)). The free energy profile of this process is shown in Figure 6, and the geometries of all implicated species are illustrated in Figure S9.

The first and second steps of phosphination with PPh₃ are similar to those of phosphination with P(OEt)₃, and their free energy barriers are 7.7 (**TS_{23/24}**) and 7.8 kcal/mol (**TS_{25/26}**), respectively. Following these steps, the NEt₃ amine abstracts a proton from C4 of the dihydropyridine intermediate **26** via the **TS_{27/28}** transition state to generate intermediate **28**. The free energy barrier of this step is 20.9 kcal/mol (relative to **26**). Subsequently, **28** isomerizes produce intermediate **29** and the S–N bond in this intermediate is broken to give the 4-phosphonato substituted pyridine **31** and an ammonium salt **14**. Considering that the aromaticity of pyridine is restored by breaking the S–N bond in **29**, the free energy barrier of this step is very small (0.4 kcal/mol). Therefore, proton abstraction (**TS_{27/28}**, 20.9 kcal/mol) is the rate-limiting step in the mechanism of 2-Ph-pyridine phosphination

with PPh_3 . The same step in the mechanism of pyridine phosphination with $\text{P}(\text{OEt})_3$ has a smaller barrier ($\text{TS}_{10/11}$, 13.0 kcal/mol) due to the relatively low steric hindrance imposed by $\text{P}(\text{OEt})_3$, whose volume is smaller than PPh_3 .

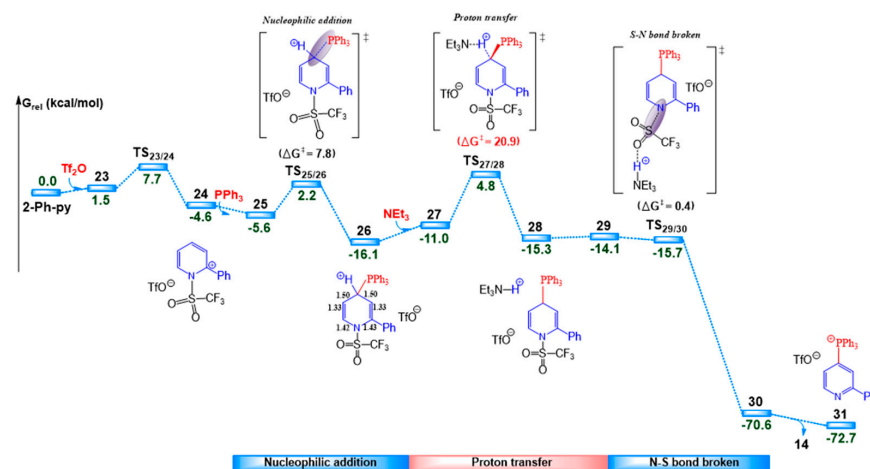


Figure 6. Free energy profile of pyridine phosphination with PPh_3 .

2.2.2. Origin of Site-Selectivity

The experiments conducted in previous studies show that the reaction of 2-Ph-pyridine phosphination with PPh_3 is highly selective and favors the formation of the para-substituted product [19,22]. To investigate the reason behind the site-selectivity of this reaction, calculations of 2-Ph-pyridine phosphination at the ortho position were performed. The obtained free energy profile is shown in Figure 7, and the geometries of all implicated species are shown in Figure S10. The nucleophilic attack of PPh_3 on the pyridinium salt **24** at the ortho position ($\text{TS}_{24/32}$) has a free energy barrier of 7.0 kcal/mol, and the barrier of the subsequent proton abstraction by NEt_3 ($\text{TS}_{32/33}$) is 22.7 kcal/mol. The latter is higher than the energy barrier of the analogous reaction, leading to the formation of the para-substituted product ($\text{TS}_{27/28}$, 20.9 kcal/mol). Based on ASM [38–40] analysis, the difference in the strain energies of the phosphonate moieties in $\text{TS}_{27/28}$ and $\text{TS}_{32/33}$ are bigger than that of the pyridine and NEt_3 moieties (Table 3). This indicates that the difference between the energies of the two transition states is mainly attributed to the phosphonate moiety. Specifically, the steric hindrance at the ortho position of pyridine renders this moiety more distorted. Therefore, the phosphination of pyridine at ortho position is less favorable than that at para position, which agrees well with the available experimental data.

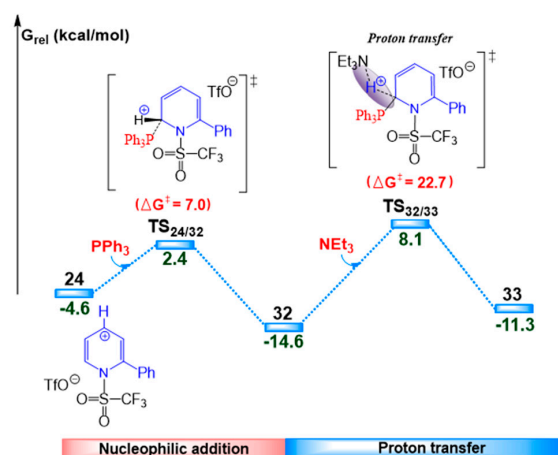


Figure 7. Free energy profile of 2-Ph-pyridine phosphination with PPh_3 to give the ortho-substituted product.

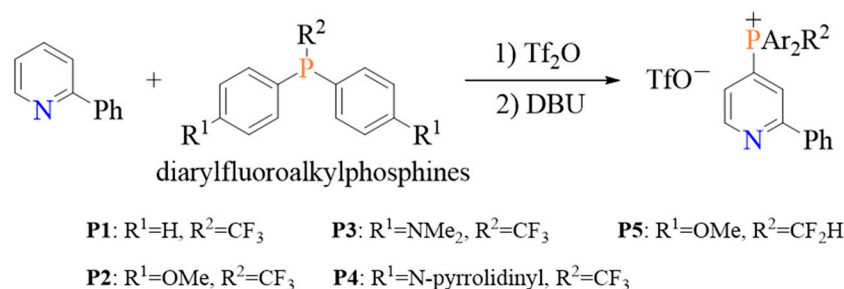
Table 3. Strain energies of pyridine, phosphonate and NEt₃ moieties in the TS_{27/28} and TS_{32/33} transition states.

	E _{strain} (kcal/mol)		
	Phosphonate	Pyridine	NEt ₃
TS _{27/28}	5.9	91	4.1
TS _{32/33}	9.1	89.6	3.2
differ	3.2	−1.4	−0.9

Overall, the results indicate that the phosphination of pyridine with PPh₃ may proceed via four successive elementary steps including activation of pyridine, nucleophilic addition, proton abstraction, and S–N bond breaking. The large volume of PPh₃ raises the free energy barrier of proton abstraction. Nevertheless, the reaction is favored by its high exothermicity (−72.7 kcal/mol). The site-selectivity is thus attributed to the unfavorable steric hindrance at the ortho position of pyridine.

2.3. Phosphination of 2-Ph-Pyridine with Diarylfluoroalkylphosphines (PAr₂CF₂X)

Paton and McNally previously reported the phosphination of 2-Ph-pyridine with diarylfluoroalkylphosphines (Scheme 2) [41]. They compared five different phosphines and found that the yield of the product correlates with the donating capacity of the phosphine's aryl substituents.

**Scheme 2.** Phosphination of 2-Ph-pyridine with diarylfluoroalkylphosphines P1–P5 using DBU as a Lewis base.

Herein, the mechanism of 2-Ph-pyridine phosphination with P1–P5 was studied and the obtained results demonstrate that unlike the phosphination reaction with PPh₃, the rate-determining step is the nucleophilic addition of phosphines. Compared to PPh₃ (proton affinity = 159.4 kcal/mol), the proton affinities of P1–P5 are smaller, as shown in Table 4. This suggests that the CF₃ and CF₂H electron-withdrawing substituents decrease the nucleophilicity of the diarylfluoroalkylphosphines, thereby increasing the energy barrier of nucleophilic addition. As a result, this reaction step becomes the rate-determining step.

Table 4. Proton affinities of P1–P5 and free energy barriers of the nucleophilic addition reactions of these phosphines to 2-Ph-pyridine.

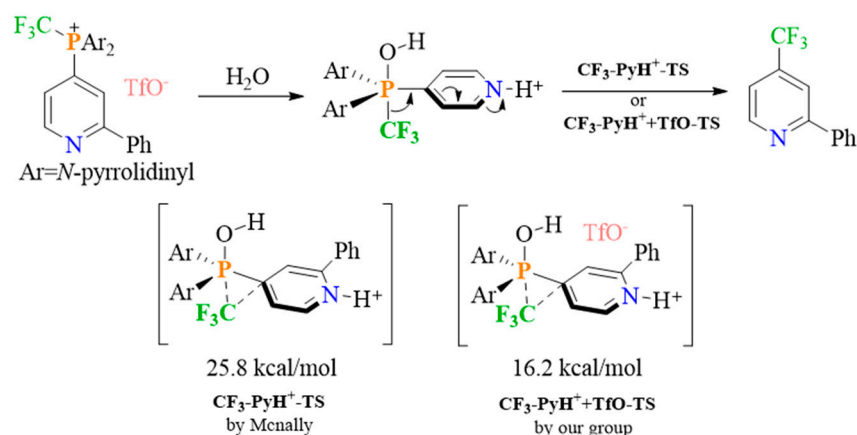
Phosphine	R ¹	R ²	Product Yield (%)	ΔG _{TS} (kcal/mol)	Protonaffinity (kcal/mol)
P1	H	CF ₃	n.d.	20.1	143.9
P2	OMe	CF ₃	54	18.2	146.6
P3	NMe ₂	CF ₃	81	12.7	153.2
P4	N-pyrrolidinyl	CF ₃	85	11.1	154.3
P5	OMe	CF ₂ H	90	11.3	153.1

Unlike the electron-withdrawing substituents (CF₃ or CF₂H) of P1–P5, the aryl electron-donating substituents (OMe, NMe₂, and N-pyrrolidinyl) promote the nucleophilicity of the phosphines, as per the proton affinity values listed in Table 4. This means that they

decrease the barrier of the nucleophilic addition elementary step. Consequently, when the aryl substituent in the diarylfluoroalkylphosphine is an electron-donating group, the nucleophilic addition of this phosphine to 2-Ph-pyridine is facile, and the product yield of the reaction is high. The opposing effects of electron-withdrawing and electron-donating substituents on the rate of 2-Ph-pyridine phosphination with diarylfluoroalkylphosphines agree well with the experimentally observed reactivities of different phosphines [41].

2.4. C-H Fluoroalkylation Reaction of 2-Ph-Pyridine

As mentioned in the introduction, the phosphonium ion can be used as a functional handle to form other chemical bonds. For example, Paton and McNally used phosphonium salts to form fluoroalkyl pyridine, and they studied this reaction both, experimentally and theoretically (DFT calculations) [41]. Based on the obtained results, the authors proposed that the reaction process involves water addition and ligand coupling, as shown in Scheme 3, and that the key transition state is the coupling of $\text{CF}_3\text{-PyH}^+$ ($\text{CF}_3\text{-PyH}^+\text{-TS}$). In the presence of TfO^- , the free energy barrier of this transition state is reduced from 25.8 to 16.2 kcal/mol, which indicates that this anion plays an important role in the $\text{CF}_3\text{-PyH}^+$ coupling reaction. Herein, the interactions in the $\text{CF}_3\text{-PyH}^+\text{-TfO-TS}$ transition state were analyzed, and as shown in Figure 8, there are two types of weak interactions: hydrogen bonding between TfO^- and OH, and dispersion effects between TfO^- and the pyridinium ring. These interactions promote ligand coupling.



Scheme 3. The fluoroalkylation of pyridine in acidic solvent starting from a phosphonium salt. $\text{CF}_3\text{-PyH}^+\text{-TS}$ is reported by Paton and McNally and $\text{CF}_3\text{-PyH}^+\text{-TfO-TS}$ is calculated by our group.

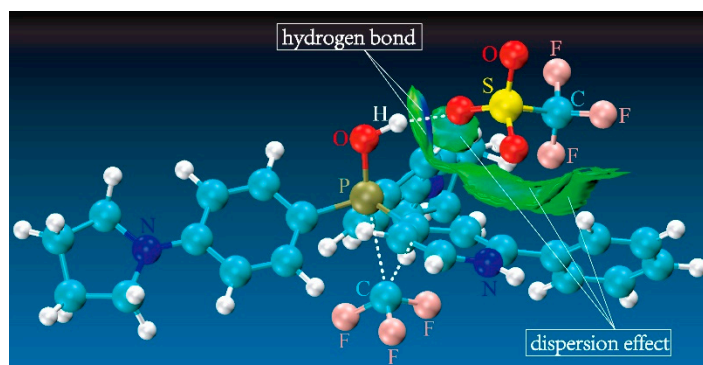


Figure 8. The weak interactions in the $\text{CF}_3\text{-PyH}^+\text{-TfO-TS}$ transition state.

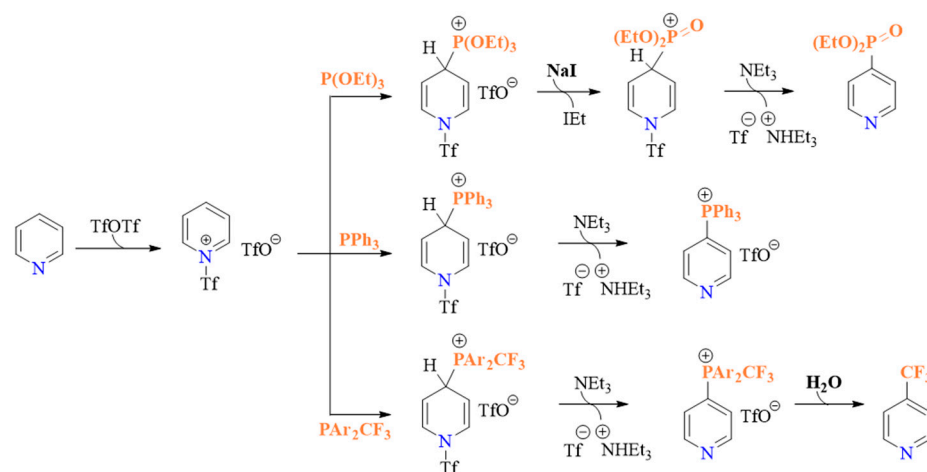
3. Computational Methods

The Gaussian16 software package [42] was used to perform all DFT calculations according to the self-consistent reaction field (SCRf) method and the IEFPCM solvation model [43], with acetonitrile as solvent. The geometries of all minima and transition states

were optimized and the harmonic frequencies calculated at the M06-2X/6-311G** level of theory in solution [44–46]. Meanwhile, single-point energy calculations of the minimum energy conformers (i.e., optimum geometries) were performed at the M06-2X/6-311++G** level of theory in solution. The 3D-optimized structures were visualized using the CYLview program [47], and the calculated frequency values were used to correct the free energy at 298.15 K and 1 atm. Based on the “the theory of free volume” [48–53], a correction factor of -2.55 (or 2.55) kcal mol^{-1} was added to the free energy values to account for the effect of the ideal gas phase model in overestimating the contribution of entropy. Meanwhile, the Gibbs energies were corrected to standard state 1 M [54]. The proton affinity were defined as the negative of the enthalpy change for the reaction ($\text{P} + \text{H}^+ \rightarrow \text{PH}^+$). The important transition states were confirmed using intrinsic reaction coordinate (IRC) analysis [55,56], and the partial atomic charges were allocated based on natural bond orbital (NBO) analyses, which were performed at the M06-2X/6-311G** level [57–59]. To study the electronic structure changes induced by the $\text{S}_{\text{N}}2$ reactions along the reaction pathway, intrinsic bond orbital (IBO) analyses were performed [60]. The weak interactions in the transition state were analyzed using the Multiwfn program [61,62].

4. Conclusions

This study uses DFT calculations to elucidate the detailed mechanism of pyridine phosphination with three different phosphines: $\text{P}(\text{OEt})_3$, PPh_3 , and PAR_2CF_3 . As shown in Scheme 4, the reactions are initiated by pyridine activation and nucleophilic addition of phosphine. In the case of phosphination with $\text{P}(\text{OEt})_3$, the subsequent steps are NaI -mediated ethyl migration and rearomatization of dihydropyridine. Meanwhile, in the case of phosphination with PPh_3 or PAR_2CF_3 , the rearomatization of dihydropyridine by NEt_3 occurs first, followed by ligand coupling of the 4-phosphonato substituted pyridine intermediate to give trifluoromethylated pyridine. Considering that the proton affinity of PAR_2CF_3 is smaller than the affinities of $\text{P}(\text{OEt})_3$ and PPh_3 , the rate-determining step of pyridine phosphination with PAR_2CF_3 is nucleophilic addition, whereas that of phosphination with $\text{P}(\text{OEt})_3$ or PPh_3 is ethyl migration and proton transfer.



Scheme 4. Summary of the possible pathways of pyridine phosphination with $\text{P}(\text{OEt})_3$, PPh_3 , and PAR_2CF_3 .

The steric hindrance of phosphine determines the site-selectivity of the phosphination reaction with $\text{P}(\text{OEt})_3$ or PPh_3 . In the case of PAR_2CF_3 , the effect of the aryl electron-donating substituents increasing the proton affinity and reducing the reaction barrier is greater than the opposing effect of the electron-withdrawing substituents, which facilitates the nucleophilic addition of the phosphine. These electronic and steric effects on the rate of the reaction further support our proposed mechanism. Finally, TfO^- plays an important role in the C–H fluoroalkylation of 2-Ph-pyridine, as it induces hydrogen bonding interactions and dispersion effects in the ligand coupling transition state.

Supplementary Materials: The following supporting information can be downloaded at: <https://www.mdpi.com/article/10.3390/molecules27175694/s1>, Figure S1: Optimized intermediates and transition states of pyridine activation and nucleophilic addition; Figure S2: Optimized intermediates and transition states of dihydropyridine rearomatization to afford the final product (path A); Figure S3: Optimized intermediates and transition states of dihydropyridine rearomatization to afford the final product (path B); Figure S4: Optimized intermediates and transition states of pyridine phosphination to afford C2-phosphonates; Figure S5: Optimized intermediates and transition states of phosphination of pyridine with P(OiPr)₃ to afford C4-phosphonates; Figure S6: Optimized intermediates and transition states of phosphination of pyridine with P(OiPr)₃ to afford C2-phosphonates; Figure S7: Free energy profile of phosphination of pyridine with P(OiPr)₃ to afford C4-phosphonates; Figure S8: Free energy profile of phosphination of pyridine with P(OiPr)₃ to afford C2-phosphonates; Table S1: Interaction and strain energies of the **iPr-p-TS**_{7/8} and **iPr-o-TS**_{7/8} transition states (unit kcal/mol); Figure S9: Optimized intermediates and transition states of pyridine phosphination with PPh₃; Figure S10: Optimized intermediates and transition states of 2-Ph-pyridine phosphination with PPh₃ to give the ortho-substituted product; Figure S11: Optimized intermediates and transition states of Phosphination of 2-Ph-pyridine with diarylfluoroalkylphosphines P1–P5; Figure S12: Optimized intermediates and transition states of The fluoroalkylation of pyridine in acidic solvent starting from a phosphonium salt; Table S2: Corrected free energies of all species; Table S3: Imaginary frequencies of all transition states; Table S4: Cartesian coordinates of all species.

Author Contributions: Conceptualization, J.Z. and P.D.; methodology, J.Z. and P.D.; software, J.Z. and P.D.; investigation, J.Z., P.D., Y.Y., D.S. and K.M.; resources, J.Z. and P.D.; data curation, P.D.; writing—original draft preparation, J.Z. and P.D.; writing—review and editing, P.D. and Q.Y.; visualization, J.Z. and P.D. All authors have read and agreed to the published version of the manuscript.

Funding: This work was supported by The Natural Science Foundation of the Jiangsu Higher Education Institutions of China (grant no. 18KJB150010, 19KJB150034), and the Qinglan Project of the Jiangsu Higher Education Institutions.

Institutional Review Board Statement: Not applicable.

Informed Consent Statement: Not applicable.

Data Availability Statement: Not applicable.

Conflicts of Interest: The authors declare no conflict of interest.

References

1. Zhao, D.; Wang, R. Recent developments in metal catalyzed asymmetric addition of phosphorus nucleophiles. *Chem. Soc. Rev.* **2012**, *41*, 2095–2108. [[CrossRef](#)] [[PubMed](#)]
2. Tan, S.-J.; Lim, J.-L.; Low, Y.-Y.; Sim, K.-S.; Lim, S.-H.; Kam, T.-S. Oxidized Derivatives of Macroline, Sarpagine, and Pleiocarpamine Alkaloids from *Alstonia angustifolia*. *J. Nat. Prod.* **2014**, *77*, 2068–2080. [[CrossRef](#)] [[PubMed](#)]
3. Fernández-Pérez, H.; Etayo, P.; Panossian, A.; Vidal-Ferran, A. Phosphine–Phosphinite and Phosphine–Phosphite Ligands: Preparation and Applications in Asymmetric Catalysis. *Chem. Rev.* **2011**, *111*, 2119–2176. [[CrossRef](#)]
4. Langer, F.; Knochel, P. A new efficient preparation of polyfunctional phosphines using zinc organometallics. *Tetrahedron Lett.* **1995**, *36*, 4591–4594. [[CrossRef](#)]
5. Peer, M.; de Jong, J.C.; Kiefer, M.; Langer, T.; Rieck, H.; Schell, H.; Sennhenn, P.; Sprinz, J.; Steinhagen, H.; Wiese, B.; et al. Preparation of chiral phosphorus, sulfur and selenium containing 2-aryloxazolines. *Tetrahedron* **1996**, *52*, 7547–7583. [[CrossRef](#)]
6. Langer, F.; Püntener, K.; Stürmer, R.; Knochel, P. Preparation of Polyfunctional Phosphines Using Zinc Organometallics. *Tetrahedron Asymmetry* **1997**, *8*, 715–738. [[CrossRef](#)]
7. Tong, W.-Y.; Ly, T.D.; Zhao, T.-T.; Wu, Y.-B.; Wang, X. Mechanism of C–P bond formation via Pd-catalyzed decarbonylative phosphorylation of amides: Insight into the chemistry of the second coordination sphere. *Chem. Commun.* **2020**, *56*, 113–116. [[CrossRef](#)]
8. Li, C.-K.; Tao, Z.-K.; Zhou, Z.-H.; Bao, X.-G.; Zhou, S.-F.; Zou, J.-P. Copper-Catalyzed Oxidative sp³-Carbon Radical Cross-Coupling with Trialkylphosphites Leading to α -Phosphonyl 1,3-Dicarbonyl Compounds. *J. Org. Chem.* **2019**, *84*, 2351–2357. [[CrossRef](#)]
9. Shan, C.; Chen, F.; Pan, J.; Gao, Y.; Xu, P.; Zhao, Y. Zn(OTf)₂-Catalyzed Phosphinylation of Propargylic Alcohols: Access to γ -Ketophosphine Oxides. *J. Org. Chem.* **2017**, *82*, 11659–11666. [[CrossRef](#)]
10. Yang, B.; Wang, Z.-X. Ni-Catalyzed C–P Coupling of Aryl, Benzyl, or Allyl Ammonium Salts with P(O)H Compounds. *J. Org. Chem.* **2019**, *84*, 1500–1509. [[CrossRef](#)]

11. Berger, O.; Montchamp, J.-L. Manganese-Mediated Intermolecular Arylation of H-Phosphinates and Related Compounds. *Chem. A Eur. J.* **2014**, *20*, 12385–12388. [[CrossRef](#)] [[PubMed](#)]
12. Hu, G.B.; Chen, W.Z.; Ma, D.M.; Zhang, Y.; Xu, P.X.; Gao, Y.X.; Zhao, Y.F. Silver-Catalyzed, Aldehyde-Induced α -C–H Functionalization of Tetrahydroisoquinolines with Concurrent C–P Bond Formation/N-Alkylation. *J. Org. Chem.* **2016**, *81*, 1704–1711. [[CrossRef](#)] [[PubMed](#)]
13. Wang, D.; Li, M.; Shuang, C.; Liang, Y.; Zhao, Y.; Wang, M.; Shi, Z. Rhodium-catalyzed selective direct arylation of phosphines with aryl bromides. *Nat. Commun.* **2022**, *13*, 2934. [[CrossRef](#)] [[PubMed](#)]
14. Tappe, F.M.J.; Trepohl, V.T.; Oestreich, M. Transition-Metal-Catalyzed C-P Cross-Coupling Reactions. *Synthesis* **2010**, *2010*, 3037–3062.
15. Chen, Y.; Yu, Z.; Jiang, Z.; Tan, J.-P.; Wu, J.-H.; Lan, Y.; Ren, X.; Wang, T. Asymmetric Construction of Tertiary/Secondary Carbon–Phosphorus Bonds via Bifunctional Phosphonium Salt Catalyzed 1,6-Addition. *ACS Catal.* **2021**, *11*, 14168–14180. [[CrossRef](#)]
16. Dmitriev, M.E.; Golovash, S.R.; Borodachev, A.V.; Ragulin, V.V. Mechanism of Phosphorus–Carbon Bond Formation in the Amidoalkylation of Phosphonous Carboxylic Acids. *J. Org. Chem.* **2021**, *86*, 593–600. [[CrossRef](#)]
17. Kwak, S.; Choi, J.; Han, J.; Lee, S.Y. Regio- and Stereoselective Addition of Secondary Phosphine Oxides to Allenates Catalyzed by Main-Group Lewis Pairs. *ACS Catal.* **2022**, *12*, 212–218. [[CrossRef](#)]
18. Akiba, K.; Negishi, Y.; Inamoto, N. A facile general synthesis of dimethyl 1-acyl-1,2-dihydroquinoline-2-phosphonates and 2-acyl-1,2-dihydroisoquinoline-1-phosphonates. *Synthesis* **1979**, *1979*, 55–56. [[CrossRef](#)]
19. Anders, E.; Markus, F. Neue Methode zur Regiospezifischen Substitution Einiger Reaktionsträger N-heteroaromatischer Ringsysteme. *Tetrahedron Lett.* **1987**, *28*, 2675–2676. [[CrossRef](#)]
20. Anders, E.; Markus, F. Chemie der Triphenyl-(oder Tri-n-butyl-)pyridylphosphoniumsalze, 1 Neue Methode zur regioselektiven Einführung von Phosphoniumgruppen in N-heteroaromatische Ringsysteme. *Chem. Ber.* **1989**, *122*, 113–118. [[CrossRef](#)]
21. Anders, E.; Markus, F. Chemie der Triphenyl-(oder Tri-n-butyl-)pyridylphosphoniumsalze, 2. 2,4-Pyridindiylibis(phosphoniumsalze). *Chem. Ber.* **1989**, *122*, 119–122. [[CrossRef](#)]
22. Haase, M.; Goerls, H.; Anders, E. Synthesis of $\text{PO}(\text{OR})_2^-$ and PR_3^+ -Disubstituted Pyridines via N-(Trifluoromethylsulfonyl)pyridinium Triflates. *Synthesis* **1998**, *1998*, 195–200. [[CrossRef](#)]
23. Haase, M.; Günther, W.; Görls, H.; Anders, E. N-Heteroarylphosphonates, Part II. Synthesis and Reactions of 2- and 4-Phosphonatoquinolines and Related Compounds. *Synthesis* **1999**, *1999*, 2071–2081. [[CrossRef](#)]
24. Hilton, M.C.; Dolewski, R.D.; McNally, A. Selective Functionalization of Pyridines via Heterocyclic Phosphonium Salts. *J. Am. Chem. Soc.* **2016**, *138*, 13806–13809. [[CrossRef](#)] [[PubMed](#)]
25. Zhang, X.; McNally, A. Phosphonium Salts as Pseudohalides: Regioselective Nickel-Catalyzed Cross-Coupling of Complex Pyridines and Diazines. *Angew. Chem. Int. Ed.* **2017**, *56*, 9833–9836. [[CrossRef](#)] [[PubMed](#)]
26. Koniarczyk, J.L.; Hesk, D.; Overgard, A.; Davies, I.W.; McNally, A. A General Strategy for Site-Selective Incorporation of Deuterium and Tritium into Pyridines, Diazines, and Pharmaceuticals. *J. Am. Chem. Soc.* **2018**, *140*, 1990–1993. [[CrossRef](#)] [[PubMed](#)]
27. Patel, C.; Mohnike, M.; Hilton, M.C.; McNally, A. A Strategy to Aminate Pyridines, Diazines, and Pharmaceuticals via Heterocyclic Phosphonium Salts. *Org. Lett.* **2018**, *20*, 2607–2610. [[CrossRef](#)]
28. Dolewski, R.D.; Fricke, P.J.; McNally, A. Site-Selective Switching Strategies to Functionalize Polyazines. *J. Am. Chem. Soc.* **2018**, *140*, 8020–8026. [[CrossRef](#)]
29. Zhang, X.; McNally, A. Cobalt-Catalyzed Alkylation of Drug-Like Molecules and Pharmaceuticals Using Heterocyclic Phosphonium Salts. *ACS Catal.* **2019**, *9*, 4862–4866. [[CrossRef](#)]
30. Dolewski, R.D.; Hilton, M.C.; McNally, A. 4-Selective Pyridine Functionalization Reactions via Heterocyclic Phosphonium Salts. *Synlett* **2018**, *29*, 8–14.
31. Hilton, M.C.; Zhang, X.; Boyle, B.T.; Alegre-Requena, J.V.; Paton, R.S.; McNally, A. Heterobiaryl synthesis by contractive C–C coupling via P(V) intermediates. *Science* **2018**, *362*, 799–804. [[CrossRef](#)] [[PubMed](#)]
32. Boyle, B.T.; Hilton, M.C.; McNally, A. Nonsymmetrical Bis-Azine Biaryls from Chloroazines: A Strategy Using Phosphorus Ligand-Coupling. *J. Am. Chem. Soc.* **2019**, *141*, 15441–15449. [[CrossRef](#)] [[PubMed](#)]
33. Jumde, R.P.; Lanza, F.; Pellegrini, T.; Harutyunyan, S.R. Highly enantioselective catalytic synthesis of chiral pyridines. *Nat. Commun.* **2017**, *8*, 2058. [[CrossRef](#)] [[PubMed](#)]
34. Wang, S.; Qiu, D.; Mo, F.; Zhang, Y.; Wang, J. Metal-Free Aromatic Carbon–Phosphorus Bond Formation via a Sandmeyer-Type Reaction. *J. Org. Chem.* **2016**, *81*, 11603–11611. [[CrossRef](#)]
35. Unoh, Y.; Hirano, K.; Miura, M. Metal-Free Electrophilic Phosphination/Cyclization of Alkynes. *J. Am. Chem. Soc.* **2017**, *139*, 6106–6109. [[CrossRef](#)]
36. Zhou, J.L.; Liu, L.; Cao, L.; Stephan, D.W. FLP reactivity of $[\text{Ph}_3\text{C}]^+$ and $(o\text{-tolyl})_3\text{P}$ and the capture of a Staudinger reaction intermediate. *Dalton Trans.* **2017**, *46*, 9334–9338. [[CrossRef](#)]
37. Du, P.; Zhao, J.; Liu, S.; Yue, Z. Insights into the nucleophilic substitution of pyridine at an unsaturated carbon center. *RSC Adv.* **2021**, *11*, 24238–24246. [[CrossRef](#)]
38. Nagase, S.; Morokuma, K. An ab initio Molecular Orbital Study of Organic Reactions. The energy, Charge, and Spin Decomposition Analyses at the Transition State and Along the Reaction Pathway. *J. Am. Chem. Soc.* **1978**, *100*, 1666–1672. [[CrossRef](#)]

39. Houk, K.N.; Gandour, R.W.; Strozier, R.W.; Rondan, N.G.; Paquette, L.A. Barriers to thermally allowed reactions and the elusiveness of neutral homoaromaticity. *J. Am. Chem. Soc.* **1979**, *101*, 6797–6802. [[CrossRef](#)]
40. Fernández, I.; Bickelhaupt, F.M. The Activation Strain Model and Molecular Orbital Theory: Understanding and Designing Chemical Reactions. *Chem. Soc. Rev.* **2014**, *43*, 4953–4967. [[CrossRef](#)]
41. Zhang, X.; Nottingham, K.G.; Patel, C.; Alegre-Requena, J.V.; Levy, J.N.; Paton, R.S.; McNally, A. Phosphorus-mediated sp^2 – sp^3 Couplings for C–H Fluoroalkylation of Azines. *Nature* **2021**, *594*, 217–222. [[CrossRef](#)] [[PubMed](#)]
42. Frisch, M.J.; Trucks, G.W.; Schlegel, H.B.; Scuseria, G.E.; Robb, M.A.; Cheeseman, J.R.; Scalmani, G.; Barone, V.; Petersson, G.A.; Nakatsuji, H.; et al. *Gaussian 16, Revision A.03*; Gaussian, Inc.: Wallingford, CT, USA, 2016.
43. Tomasi, J.; Mennucci, B.; Cammi, R. Quantum Mechanical Continuum Solvation Models. *Chem. Rev.* **2005**, *105*, 2999–3094. [[CrossRef](#)]
44. Zhao, Y.; Truhlar, D.G. Density Functionals with Broad Applicability in Chemistry. *Acc. Chem. Res.* **2008**, *41*, 157–167. [[CrossRef](#)] [[PubMed](#)]
45. Zhao, Y.; Truhlar, D.G. The M06 suite of density functionals for main group thermochemistry, thermochemical kinetics, noncovalent interactions, excited states, and transition elements: Two new functionals and systematic testing of four M06-class functionals and 12 other functionals. *Theor. Chem. Acc.* **2008**, *120*, 215–241.
46. Krishnan, R.; Binkley, J.S.; Seeger, R.; Pople, J.A. Self-consistent molecular orbital methods. XX. A basis set for correlated wave functions. *J. Chem. Phys.* **1980**, *72*, 650–654. [[CrossRef](#)]
47. Legault, C.-Y. *CYLVIEW, Version 1.0 b*; Université de Sherbrooke: Sherbrooke, QC, Canada, 2009. Available online: <https://www.cylvview.org> (accessed on 9 August 2022).
48. Benson, S.-W. *The Foundations of Chemical Kinetics*; McGraw-Hill: New York, NY, USA, 1960.
49. Okuno, Y. Theoretical Investigation of the Mechanism of the Baeyer–Villiger Reaction in Nonpolar Solvents. *Chem. A Eur. J.* **1997**, *3*, 212–218. [[CrossRef](#)]
50. Liu, Q.; Lan, Y.; Liu, J.; Li, G.; Wu, Y.-D.; Lei, A. Revealing a Second Transmetalation Step in the Negishi Coupling and Its Competition with Reductive Elimination: Improvement in the Interpretation of the Mechanism of Biaryl Syntheses. *J. Am. Chem. Soc.* **2009**, *131*, 10201–10210. [[CrossRef](#)]
51. Schoenebeck, F.; Houk, K.N. Ligand-Controlled Regioselectivity in Palladium-Catalyzed Cross Coupling Reactions. *J. Am. Chem. Soc.* **2010**, *132*, 2496–2497. [[CrossRef](#)]
52. Liu, B.; Gao, M.; Dang, L.; Zhao, H.; Marder, T.B.; Lin, Z. DFT Studies on the Mechanisms of the Platinum-Catalyzed Diboration of Acyclic α,β -Unsaturated Carbonyl Compounds. *Organometallics* **2012**, *31*, 3410–3425. [[CrossRef](#)]
53. Zhao, J.; Liu, S.; Liu, S.; Ding, W.; Liu, S.; Chen, Y.; Du, P. A Theoretical Study on the Borane-Catalyzed Reductive Amination of Aniline and Benzaldehyde with Dihydrogen: The Origins of Chemoselectivity. *J. Org. Chem.* **2022**, *87*, 1194–1207. [[CrossRef](#)]
54. Alvarez-Idaboy, J.R.; Reyes, L. Reinvestigating the Role of Multiple Hydrogen Transfers in Baeyer–Villiger Reactions. *J. Org. Chem.* **2007**, *72*, 6580–6583. [[CrossRef](#)] [[PubMed](#)]
55. Fukui, K. The path of chemical reaction—The IRC approach. *Acc. Chem. Res.* **1981**, *14*, 363–368. [[CrossRef](#)]
56. Hratchian, H.P.; Schlegel, H.B. Finding minima, transition states, and following reaction pathways on ab initio potential energy surfaces. In *Theory and Applications of Computational Chemistry: The First Forty Years*; Dykstra, C.E., Frenking, G., Kim, K.S., Scuseria, G.E., Eds.; Elsevier: Amsterdam, The Netherlands, 2005; pp. 195–249.
57. Wiberg, K. Application of the pople-santry-segal CNDO method to the cyclopropylcarbinyl and cyclobutyl cation and to bicyclobutane. *Tetrahedron* **1968**, *24*, 1083–1096. [[CrossRef](#)]
58. Reed, A.E.; Curtiss, L.A.; Weinhold, F. Intermolecular interactions from a natural bond orbital, donor-acceptor viewpoint. *Chem. Rev.* **1988**, *88*, 899–926. [[CrossRef](#)]
59. Weinhold, F. Natural bond orbital analysis: A critical overview of relationships to alternative bonding perspectives. *J. Comput. Chem.* **2012**, *33*, 2363–2379. [[CrossRef](#)]
60. Knizia, G.; Klein, J.E.M.N. Electron Flow in Reaction Mechanisms—Revealed from First Principles. *Angew. Chem. Int. Ed.* **2015**, *54*, 5518–5522. [[CrossRef](#)] [[PubMed](#)]
61. Lu, T.; Chen, F. Multiwfn: A multifunctional wavefunction analyzer. *J. Comput. Chem.* **2012**, *33*, 580–592. [[CrossRef](#)]
62. Lu, T.; Chen, Q. Independent Gradient Model Based on Hirshfeld Partition: A New Method for Visual Study of Interactions in Chemical Systems. *J. Comput. Chem.* **2022**, *43*, 539–555. [[CrossRef](#)]